Hindawi
Mathematical Problems in Engineering
Volume 2019, Article ID 4897156, 14 pages
https://doi.org/10.1155/2019/4897156

Research Article

Research and Economic Analysis of the Source-Load Coordination of Oil Shale Exploitation

Xiyun Yang,[1,2] Le Zhang,[1] Tianze Ye,[2] Yuwei Yang,[2] Yiwei Wang,[1] and Jianzheng Su[1]

[1]*State Energy Center for Shale Oil Research and Development, Haidian District, Beijing 100083, China*
[2]*School of Control and Computer Engineering, North China Electric Power University, Beijing, China*

Correspondence should be addressed to Tianze Ye; yetianze613@163.com

Received 5 August 2019; Revised 2 October 2019; Accepted 10 October 2019; Published 31 October 2019

Academic Editor: Hao Zhang

In-situ exploitation of oil shale by electric heating consumes large amounts of electricity. Under the existing dispatch system, using wind power output and photovoltaic power output to support the exploitation of oil shale can promote renewable energy use, reduce the consumption of coal and other fossil fuels, and protect the environment from pollution. In this study, the characteristics of the wind power and photovoltaic power output are analyzed, and the correlation between the power outputs is evaluated using the copula function. The load of exploiting oil shale is presented. In order to match the heating load characteristics of oil shale exploitation, a particle swarm optimization algorithm is used to optimize the heating temperature of the heated well to minimize the cost. An economic analysis is conducted of five different power supply combinations, including wind power, photovoltaic power, and the existing power grid. The income ratio of the five modes is calculated using actual data of a project in Jilin province in China, and the feasibility of in-situ electric heating by wind power, photovoltaic power, and the power grid is determined. The results of this study provide useful references for decision makers to plan the power supply scheme for in-situ oil shale exploitation.

1. Introduction

Oil shale is a fossil fuel with high ash content and low calorific value that contains organic matter insoluble in ordinary solvents. After low-temperature dry distillation, oil shale, dry distillation gas, and shale semicoke are obtained. China's oil shale has a history of more than 70 years and has been mainly used for refining and power generation. In 2006, the shale oil production exceeded 200,000 t in Fushun in Liaoning province, Maoming in Guangdong province, Huadian and Wangqing in Jilin province, Longkou in Shandong province, and Tanshanling in Gansu province [1].

In the early stage of oil shale exploitation, surface exploitation is the main method and surface dry distillation is used to obtain shale oil and its by-products. These mining methods pollute the soil, vegetation, water, and air. In order to develop cleaner mining methods and reduce environmental pollution, scholars have focused on in-situ exploitation of oil shale. In in-situ underground mining, well drilling and heat injection are used to heat the underground oil shale layer, and the shale gas or shale oil is obtained by pyrolysis of the underground rock layer; subsequently, the oil and gas are recovered through the production well. Unlike surface mining, the in-situ mining method does not require mining stone and transportation nor does it require the construction of ground distillation equipment and a large exhaust gas treatment device [2]. Moreover, since in-situ combustion is not restricted by the depth of the formation, it can be used to extract oil and gas from deeper and thicker oil shale layers.

There are three types of the in-situ oil shale production method according to the heating modes: electric heating, convection heating, and radiation heating. In electric heating, the heating rod heats the oil shale layer by heat conduction [3] to achieve kerogen pyrolysis, and the produced oil and gas are obtained by condensation [4–6]. In convection heating, high-temperature steam or hydrocarbon gas is injected into the oil shale layer. The high-temperature

fluid increases the temperature of the oil shale layer due to thermal convection and thermal conduction of the oil shale, and oil and gas are generated through pyrolysis [7, 8]. In convection heating, the fluid is not easily controlled and short circuits may occur; in addition, a large amount of water may be needed, which results in environmental pollution [3]. The method of heating oil shale by microwaves emitted by microwave generators is called radiation heating. This method has fast heat transfer speed, good heating performance, and high oil recovery rate and selectively heats the oil shale layer. However, the cost and technical difficulty of this method are very high. To sum up, it is very important to develop an in-situ method for oil shale exploitation that has low cost, high efficiency, and relatively low pollution. If a sustainable and more economical power source can be found to provide energy for electrically heated in-situ oil shale extraction, the cost of the extraction technology can be lowered.

Renewable energy sources such as wind and photovoltaic power have many advantages, such as no pollution and sustainability and, therefore, have a broad development prospect. However, their output is characterized by being intermittent, volatile, and random, which results in challenges to develop optimal dispatch strategies in the power grid [9–12]. Scholars at home and abroad have conducted much research on the optimal scheduling of wind power or photovoltaic power systems. However, in the past five years of wind power development, two phenomena have been observed: (1) the "good news" that the wind power installed capacity continues to increase and (2) the "curtailed wind" dilemma caused by insufficient consumption ability. This has become a significant symbol of the development of new energy in China in the previous period [13]. From 2011 to the first half of 2015, the total wind power online capacity was 561.774 billion kW·h, and the total curtailed wind power was 80.191 billion kW·h. The average curtailed wind power comprised 14.27%; in the first half of 2015, the national average curtailed wind power comprised 15.17%, and the curtailed wind power of Jilin province was a record of 42.96%, followed by that of Gansu province at 30.98% and that of Xinjiang at 28.82%, indicating that the development of China's wind power experienced an electricity dilemma [14–16]. After 2012, China's installed photovoltaic capacity began to grow rapidly, and in 2014, consumption problems caused by this rapid growth began to appear, and the problem of curtailed photovoltaic power attracted the attention of the general population. According to the "Brief Information on Photovoltaic Power Generation from January to September 2015" released by the National Energy Administration, the cumulative photovoltaic power generation from January to September was 30.6 billion kW·h, and the photovoltaic power consumption was about 3 billion kW·h; the curtailed photovoltaic power accounted for 10%. Photovoltaic power is mainly generated in the Gansu and Xinjiang regions, and in many cases, photovoltaic power generation in China has been abandoned [17].

Since the first wind farm was built in Jilin province in 1999, wind power has been developing rapidly, and the installed capacity has been increasing rapidly every year. However, due to the influence of regional economic growth and the power installation structure, curtailed wind power and power rationing has become a considerable problem in wind power projects since 2011. In addition to ranking third among all provinces in 2011, the proportion of curtailed wind power and power rationing ranked first in all provinces in 2012, 2013, and 2014. The harnessing of wind and photovoltaic power and the energy distribution have become considerable problems. Bie et al. [18] proposed an optimal scheduling strategy for wind power consumption through demand-side response technology, which reduced the operating cost of the system. Jia-yun [19] used the cosine similarity between the total wind-solar storage output curve and the planned output curve as the objective function and proposed an optimal control method for energy storage based on stochastic opportunity programming. This method ensured that the energy storage device was appropriate for the output of the wind-solar hybrid system. At present, scholars at home and abroad have mainly investigated optimal scheduling strategies for wind power and photovoltaic power systems from the perspective of source-load interaction and energy storage devices suitable for the wind output so that the systems can be adapted to large-scale access to renewable energy by regulating loads in a flexible manner or dispatching charging and discharging power of the energy storage device [20–23]. Riboldi and Nord [24] optimized the operating cost and pollutant emission cost of conventional units and established an optimal power dispatch model based on "source-grid-load-storage" coordination, but the model only considered the entire consumption of wind and photovoltaic power. The "Load" and "Storage" were only used to reduce the operating cost of the conventional units without considering the high permeability of renewable energy, and the phenomenon of curtailed wind and solar power and its effect on the improvement of wind and photovoltaic power accommodation were not considered [25]. Wang et al. [26] focused on the problem of curtailed wind and solar power in China and proposed the real-time synchronous accommodation of load-grid-source coordination and an evaluation method of real-time accommodation of curtailed wind and solar power. However, wind or solar energy is not being used to extract shale oil.

In order to fill this research gap, in this paper, a study and economic analysis on the wind power/photovoltaic output/load coordination of oil shale exploitation are presented. First, the power characteristics of wind power generation, photovoltaic power generation, and the exploitation load of oil shale in the Jilin area are analyzed to provide useful references for decision makers to plan the power supply scheme and scale of oil shale exploitation. Then, an economic analysis of five power supply schemes for oil shale for the load power supply is conducted. When the oil shale is heated to 450°C, the yield of the shale oil is 90%. We use the approach of heating the oil shale to 450°C, followed by cooling and reheating to 450°C, and we develop a dispatch strategy of wind-solar-grid coordination. Particle swarm optimization (PSO) is used to optimize the heating temperature of the well, and the optimal reheating temperature

and power supply cost of the heated well are obtained by using the lowest cost as determined by an objective function. An economic analysis is conducted using actual data from a project in Jilin province in China, and the profits and the electricity cost for the five power supply methods are determined. The results provide references for researchers to formulate optimal dispatch strategies for the power supply.

2. The Characteristics of Wind Power

2.1. Seasonal Characteristics. Probability and statistical analyses were used to analyze the seasonal characteristics of the wind power output in a certain area of Northwest China. The annual utilization hours of wind power are 1671 h. The average output ratio of the wind power is between 0.141 and 0.260; the largest value and smallest value were observed in March and May, respectively. The average output ratio in spring, summer, autumn, and winter were 0.201, 0.163, 0.194, and 0.203, respectively. Overall, the wind power exhibits a larger output in spring and winter and a smaller output in summer and autumn.

2.2. Probability Distributions

2.2.1. Full-Time Wind Power Output Ratio: Probability Statistics. The statistical results of the probability distribution and cumulative probability distribution are shown in Figure 1. The probability of the wind power output is largest in the range of 0~0.05, accounting for about 43%. Except for a small peak in the interval of 0.1~0.15, the probability decreases with the increase in the wind power output. The cumulative probability curve of the full-time wind power output is characterized by a convex quadratic function. At 0.3, the cumulative probability exceeds 95%.

2.2.2. Probability Statistics for Different Time Periods. The probability distribution and cumulative probability distribution at different hours during the day/night are shown in Figure 2.

The output probability and cumulative probability of the wind power output are similar for the different time periods. The probability of the wind power output is largest for 0~0.50, accounting for more than 35%. The probability of the remaining output intervals is less than 20%.

3. The Characteristics of Photovoltaic Power

Probability and statistical analyses were used to analyze the characteristics of the photovoltaic power output. The data represent output data (every 5 min) of typical photovoltaic power stations in a certain area in Northwest China in a certain year. The photovoltaic power output in the night time was zero, and only the data for the daytime (6 : 00~19 : 00) were statistically analyzed. Using the historical data and the planned installed capacity and distribution, a simulation analysis of the annual output characteristics was conducted. In order to make better comparative analysis, the data are normalized. The calculation method is as follows: $\alpha = P_{pva}/P_{pvr}$, where P_{pva} is the actual photovoltaic output power of the photovoltaic power station, MW; P_{pvr} is the rated installed power of the photovoltaic power station, MW; and α is the normalized value. It should be noted that the photovoltaic and wind power output characteristics analyzed in this study are affected by the sample selection, and the results may not be applicable to other regions but the analysis methods are generally applicable.

3.1. Seasonal Characteristics. The annual utilization hours of photovoltaic generation in the region were 2573 h, and the average monthly output was between 0.025 and 0.107, as shown in Figure 3. The average output is largest in July and smallest in January. The average outputs of photovoltaic power in the spring, summer, autumn, and winter are 0.3018, 0.3765, 0.2251, and 0.0966, respectively. Overall, the seasonal characteristics of the photovoltaic power indicate that the output is larger in spring and summer and lower in autumn and winter.

3.2. Daily Characteristics

3.2.1. Daily Maximum Output. Table 1 shows that the distribution of the maximum daily output in the region is normally distributed; the range is (0.2, 0.9), and the maximum daily output for the year is 0.902. The minimum daily output for the year is 0.195, which does not reach the rated output. The daily maximum output is lower in the winter than in the spring, summer, and autumn.

3.2.2. Daily Characteristics. The photovoltaic outputs on a sunny day and cloudy day are shown in Figure 4. The shape of the curve of the photovoltaic power output on a sunny day is similar to sine half wave; the curve is very smooth, and the output time range is 6 : 00~19 : 00; the maximum value occurs at noon. The power output on a cloudy day is affected by cloud cover, and the irradiance changes greatly, resulting in large fluctuations of the photovoltaic power output.

3.3. Probability Distributions

3.3.1. Full-Time Photovoltaic Power Output Ratio: Probability Statistics. The output probability and cumulative probability of the photovoltaic power output are shown in Figure 5. The curve is smooth, showing a small output, a large probability of intermediate output, and a small probability of large output. The annual maximum output of the photovoltaic power is 0.902, the probability of an output greater than 0.75 is 0.24%, and the probability of an output less than 0.15 is 76.55%. The cumulative probability of an output less than 0.75 is 99.76%, and the cumulative probability of a photovoltaic output less than 65% is 98.9%.

3.3.2. Probability Distribution and Cumulative Probability Distribution Curve for Different Time Periods. The probability distribution and cumulative probability distribution at different hours during the day are shown in Figure 6; the

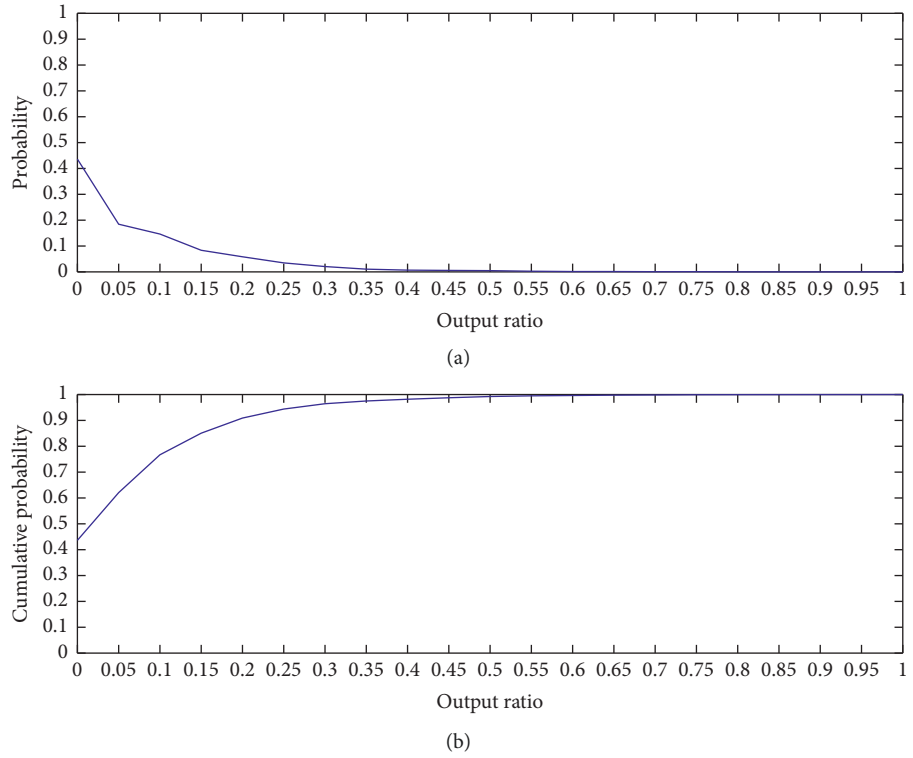

Figure 1: Output probability and cumulative probability of the wind power output.

output at 12 : 00, 13 : 00, and 14 : 00 is large, and the output curves are similar.

4. Correlation Model of Wind Power and Photovoltaic Output

4.1. Copula Theory. Sklar's theorem describes the relationship between a multivariate distribution and copula functions and can construct multivariate distribution function by copula function and edge distribution and then solve the problem of multivariate joint distribution [27].

Sklar's theorem is as follows [28]: if $H(\cdot,\cdot)$ is the joint distribution function of the marginal distribution $F(\cdot)$ and $G(\cdot)$, then there exists a copula function $C(\cdot,\cdot)$ that satisfies

$$H(x, y) = C(F(x), G(y)). \tag{1}$$

By using the density function $C(\cdot,\cdot)$ of the copula function $c(\cdot,\cdot)$ and the marginal distribution function $F(\cdot)$ and $G(\cdot)$, the density function of the distribution function $H(x, y)$ can be obtained:

$$h(x, y) = c(F(x), G(y)) \cdot f(x) \cdot g(y), \tag{2}$$

where $c(u, v) = \partial C(u, v)/\partial u\,\partial v$, $u = F(x)$; $v = G(y)$, and $f(\cdot)$ and $g(\cdot)$ are density functions of the edge distribution functions $F(\cdot)$ and $G(\cdot)$, respectively.

4.2. Correlation Analysis of Wind-Solar Power Output. Based on the natural complementary characteristics of the wind-solar power output and the ability of the Frank copula function to describe the negative correlation between variables, the Frank copula function was used as the connection function of the joint probability distribution of the wind and photovoltaic power station outputs.

The distribution function and density function of the Frank copula function are as follows:

$$C_F(u, v; \lambda) = -\frac{1}{\lambda}\ln\left(1 + \frac{\left(e^{-\lambda u} - 1\right)\left(e^{-\lambda v} - 1\right)}{e^{-\lambda} - 1}\right), \tag{3}$$

$$c_F(u, v; \lambda) = \frac{-\lambda\left(e^{-\lambda} - 1\right)e^{-\lambda(u+v)}}{\left[\left(e^{-\lambda} - 1\right) + \left(e^{-\lambda u} - 1\right)\left(e^{-\lambda v} - 1\right)\right]^2}, \tag{4}$$

where λ is the relevant parameter, $\lambda \neq 0$. $\lambda > 0$ means that the random variables u and v are positively correlated, $\lambda \longrightarrow 0$ means that the random variables u and v tend to be independent, and $\lambda < 0$ means that the random variables u and v are negatively correlated.

The correlation measure of the copula function reflects the correlation between the random variables under strictly monotonically increasing transformation. If the trend of the two random variables is the same, then they are positively correlated. If the two random variables have opposite trends, they are negatively correlated. The consistency-based Kendall rank correlation coefficient is defined as

$$\tau \equiv P\left[\left(x_1 - x_2\right)\left(y_1 - y_2\right) > 0\right] - P\left[\left(x_1 - x_2\right)\left(y_1 - y_2\right) < 0\right], \tag{5}$$

where (x_1, y_1) and (x_2, y_2) are independent identically distributed random vectors.

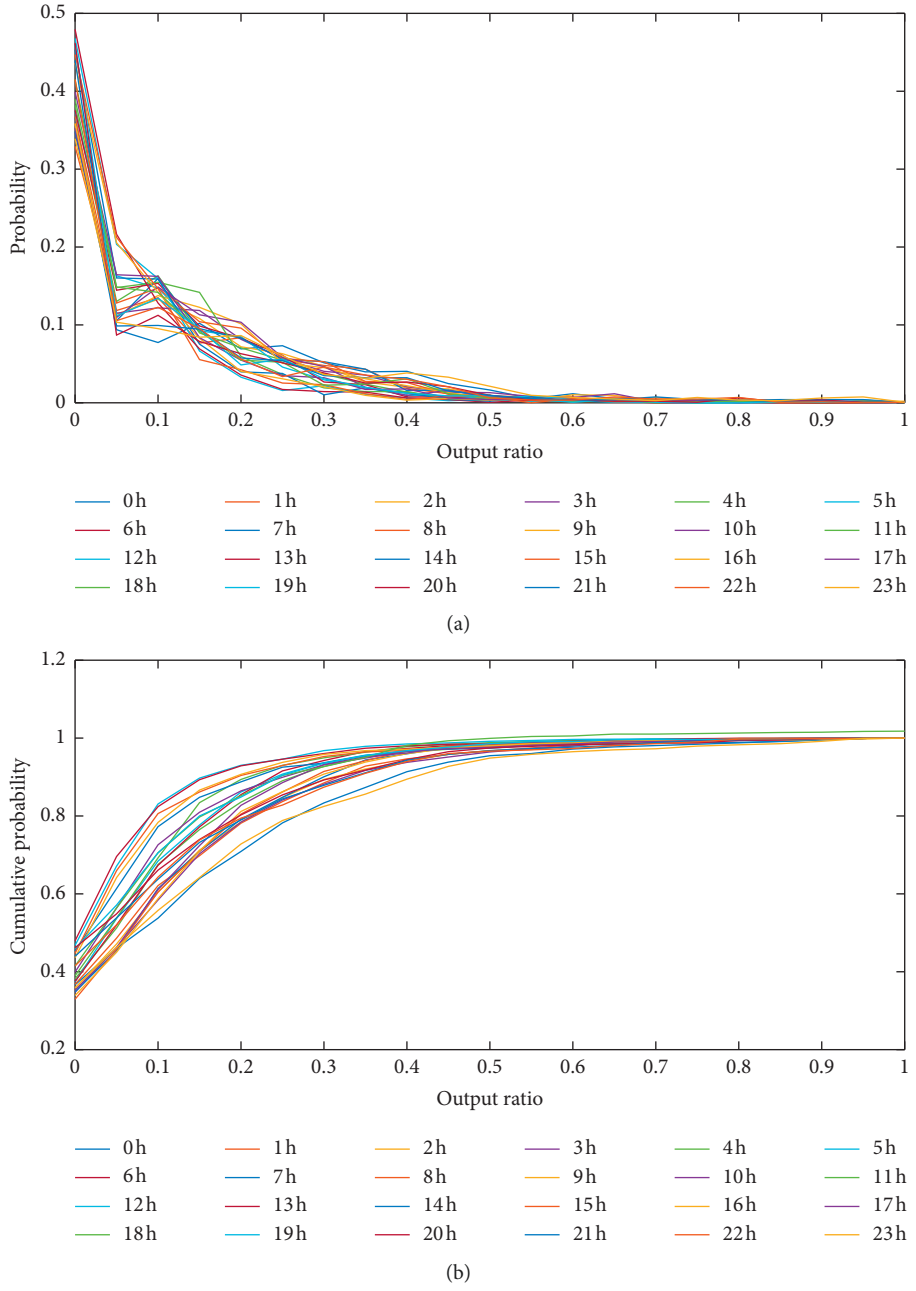

Figure 2: Output probability and cumulative probability for different time periods.

The correlation parameter λ of the Frank copula function has a one-to-one correspondence with the consistency-based correlation measure. The relationship between the Kendall rank correlation coefficient τ and the correlation parameter λ is

$$\tau = 1 + \frac{4}{\lambda}\left[D_k(\lambda) - 1\right], \tag{6}$$

where $D_k(\lambda) = (k/\lambda^k)\int_0^\lambda (t^k/e^t - 1)\mathrm{d}t$, $k = 1$.

Based on the copula theory, the correlation model of the wind-solar power output is established; the steps to obtain the joint probability distribution of the wind-solar power output are as follows:

(1) Obtain the output sample sets P_{WTG} and P_{PVG} of the wind farms and photovoltaic power stations.

(2) According to the sample sets P_{WTG} and P_{PVG}, the probability density function sum of the wind farms and photovoltaic power stations is obtained.

(3) According to $f(P_{\mathrm{WTG}})$ and $f(P_{\mathrm{PVG}})$, the marginal distribution functions $F(P_{\mathrm{WTG}})$ and $F(P_{\mathrm{PVG}})$ of the wind farm and photovoltaic power station are obtained.

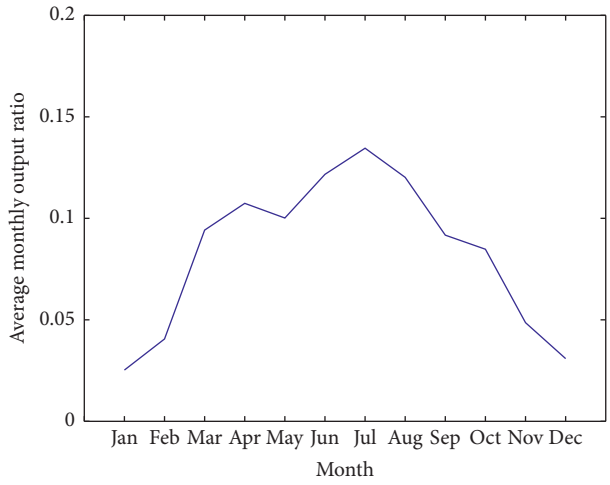

Figure 3: Monthly average power output of photovoltaic power.

Table 1: Maximum daily power output of photovoltaic power.

Extrema	Annual	Spring	Summer	Autumn	Winter
Maximum	0.902	0.874	0.902	0.783	0.479
Minimum	0.195	0.263	0.381	0.201	0.195

(4) The sample sets P_{WTG} and P_{PVG} are substituted into equation (5) to calculate the Kendall rank correlation coefficient τ of the wind farms and photovoltaic power stations.

(5) Substitute τ into equation (6) to calculate the relevant parameter λ.

(6) The wind-solar power output correlation model based on equations (2) and (4) is obtained, namely, the joint probability distribution of the wind power plant and the photovoltaic power station output:

$$h(P_H) = h(P_{\mathrm{WTG}}, P_{\mathrm{PVG}}) = \frac{-\lambda(e^{-\lambda}-1)e^{-\lambda(u+v)}f(P_{\mathrm{WTG}})f(P_{\mathrm{PVG}})}{\left[(e^{-\lambda}-1)+(e^{-\lambda u}-1)(e^{-\lambda v}-1)\right]^2}, \quad (7)$$

where P_H is the wind-solar combined output ratio, $u = F(P_{\mathrm{WTG}})$, and $v = F(P_{\mathrm{PVG}})$.

According to the joint probability distribution of the combined output of the wind farm and photovoltaic power station, the distribution function is obtained as follows:

$$H(P_H) = H(P_{\mathrm{WTG}}, P_{\mathrm{PVG}}) = \iint_{W_{\mathrm{WTG}}P_{\mathrm{WTG}}+W_{\mathrm{PVG}}P_{\mathrm{PVG}}\le P_H} h(P_{\mathrm{WTG}}, P_{\mathrm{PVG}})dP_{\mathrm{WTG}}d_{\mathrm{PVG}}, \quad (8)$$

where W_{WTG} is the installed capacity of the wind farm and W_{PVG} is the installed capacity of the photovoltaic power station.

The Kendall rank correlation coefficient τ and correlation parameter λ for the different seasons obtained from the data of P_{WTG} and P_{PVG} of a certain region in Jilin province are shown in Table 2. The joint probability distribution of the wind power and photovoltaic power output based on the wind-solar power output correlation model is shown in Figure 7.

As shown in Figure 7 and Table 2, the rank correlation coefficient τ and the correlation parameter λ of the seasons are close to 0, and the wind power output and photovoltaic power output are not correlated. The Frank copula function describes the correlation of the wind power and photovoltaic power output. The correlation model of the wind-solar power output based on the copula function shows that the correlation characteristics between the wind farm and photovoltaic station power output in this area are not obvious.

5. Load Characteristics

5.1. Large-Scale Oil Shale Mining. In the target area, 20 horizontal wells were drilled, and they were divided into heated wells and production wells. The distance between the heated wells was 10 m, as shown in Figure 8. The horizontal well section was 500 m long, and the heating power [4] was 1 kW/m. The heating power was calculated as follows: $1\,\mathrm{kW/m} * 500\,\mathrm{m} * 18 * 1\,h = 9000\,\mathrm{kW\,h}$. As shown in Figure 9, this paper uses wind and photovoltaic energy to provide electricity for oil shale in-situ mining [29]. The electricity generated by wind farms and photovoltaic power stations is transported from the grid to the mining area. Two horizontal heating wells are separated by ten meters. The heating rod is placed horizontally in the oil shale layer. The conductive device is connected to the positive pole of the power supply; the end of the heating rod is connected, and the negative pole is connected through a conductive device. This creates a simple electrical configuration. These electric heaters convert electrical energy into thermal energy, heating the formation in the form of conduction and convective radiation. When the temperature reaches a certain high value, the organic matter in the oil shale begins to transform into shale oil.

5.1.1. Load Calculation Method. The exploration of the oil shale deposits in the study area in Jilin province shows that the oil shale is located 372~380 m below ground. The local annual average temperature is 4.5°C, the geothermal gradient is 2.5°C/100 m, and we set the Jilin surface temperature to 12°C. The relationship between the oil production rate of the oil shale and the heating temperature is shown in Figure 10.

The oil shale starts to produce oil at a temperature of 350°C. At 400°C, the shale oil yield is 40%, and at 450°C, the shale oil yield is 90%. For optimization, an intermittent heating method is used with the following steps: (1) the oil shale is heated to a temperature of 450°C; (2) this is followed by cooling; and (3) the oil shale is reheated to 450°C. PSO is used to determine the optimal temperature to minimize the electricity cost. If the initial cooling temperature in step 2 is 400°C, the oil shale yield is assumed to be constant during the cooling process. For the two large-scale oil shale targets,

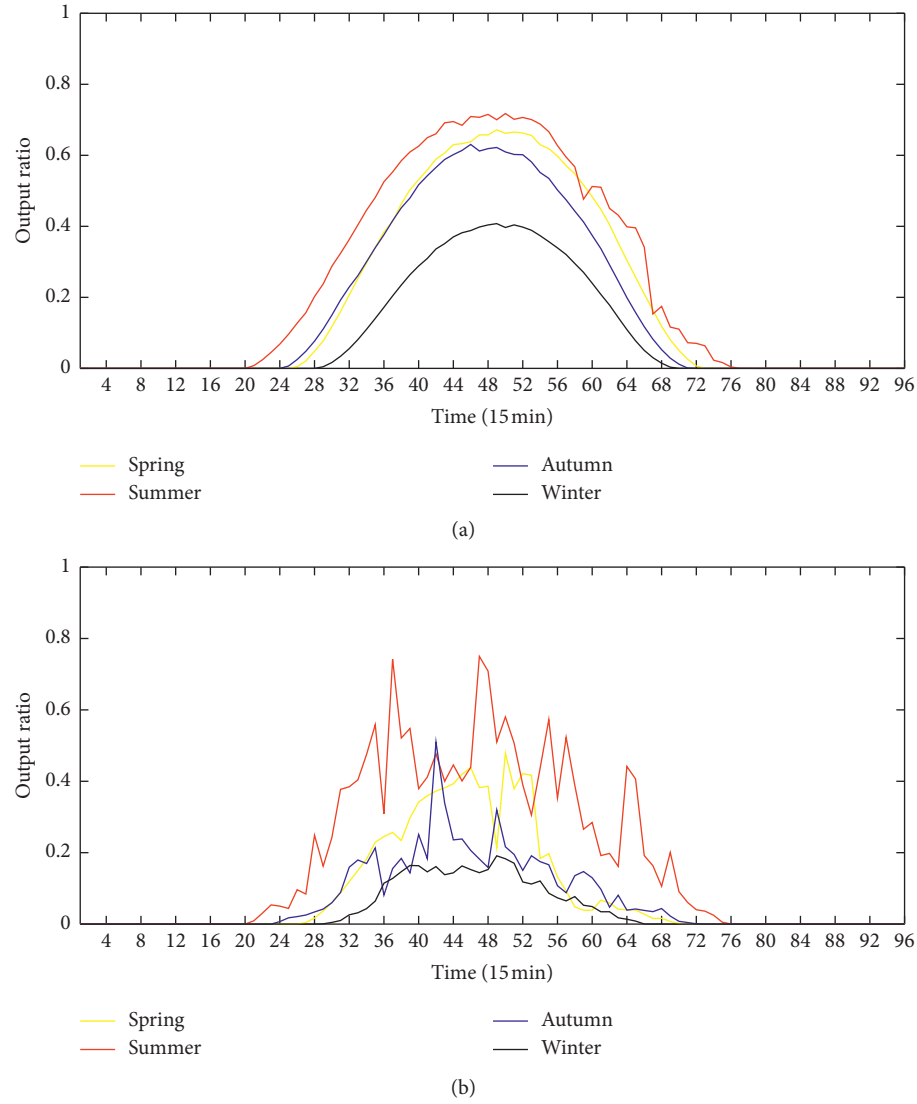

Figure 4: Daily power output characteristic of photovoltaic power on (a) a sunny day and (b) a cloudy day.

the electricity consumption is 9000 kW/h, and the oil yield is 98910 tons. We assume that the heat absorption efficiency values are 0.7 and 0.6, respectively.

The heat [30] is calculated as

$$Q = C \cdot M \cdot \Delta t, \tag{9}$$

where C is the specific heat capacity of the oil shale (2000 J/(kg·°C)); M is the heating quality, $M = \rho V = 7.85 * 10^7$ (kg); Δt is the heating time; $\Delta t_1 = 450 - 12 = 438$ (h); and $\Delta t_2 = \Delta t_3 = 450 - 400 = 50$ (h).

The heating index is shown in Table 3.

As shown in Table 3, when the heating efficiency is 0.7, the time required to increase the temperature by 1°C is 6.92 h, and the time required to decrease the temperature by 1°C is 16.15 h; when the heating efficiency is 0.6, the time required to increase the temperature by 1°C is 8.08 h and the time required to decrease the temperature by 1°C is 12.11 h.

The output probability and cumulative probability of the photovoltaic power are shown in Figure 6. The curves are symmetric around the time of 13 : 00. The output at 12 : 00, 13 : 00 and 14 : 00 are large, and the output curves are similar.

5.1.2. Load Power Curve. As the temperature rises, the power consumption is 9000 kW/h. The power fluctuation range is 2%, and the load power curve is shown in Figure 11. The main reasons are as follows:

(1) A characteristic of formation temperature propagation is that the temperature changes with the depth. According to the literature, the oil shale in Jilin province is located at a depth of 300–400 m, and the temperature increases by 2.5°C for every 100 m of depth. The time required for temperature propagation has to be considered during the heating process. When electric heating is used for shale oil extraction, 9000 kW/h cannot be maintained.

(2) Interference and heat dissipation will occur during the heating process. We used horizontal well heating,

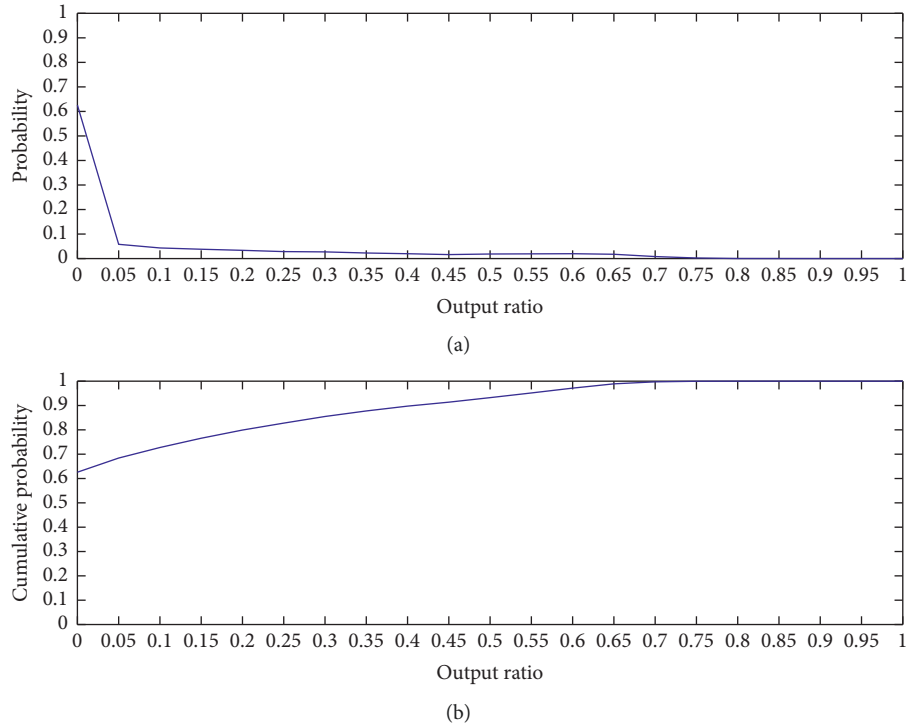

Figure 5: Output probability and cumulative probability of the photovoltaic power output.

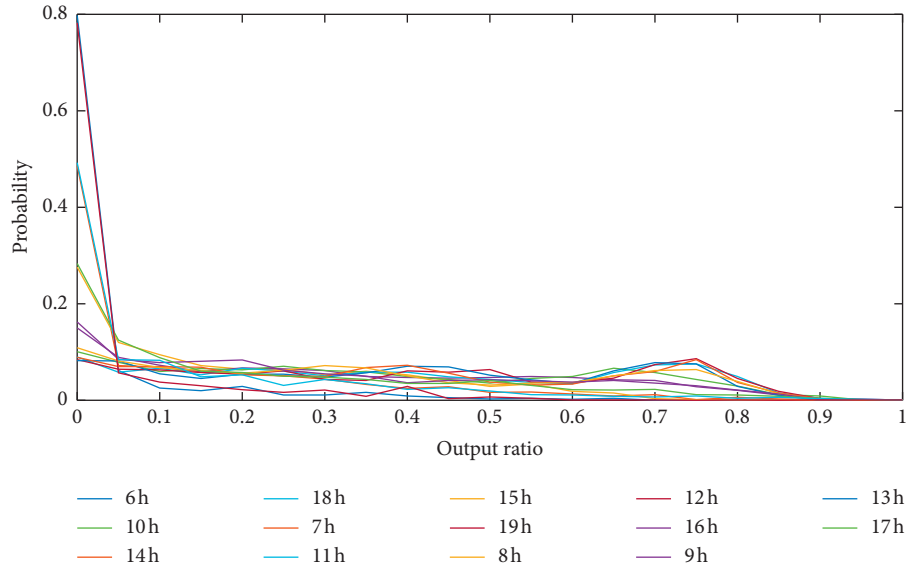

(a)

Figure 6: Continued.

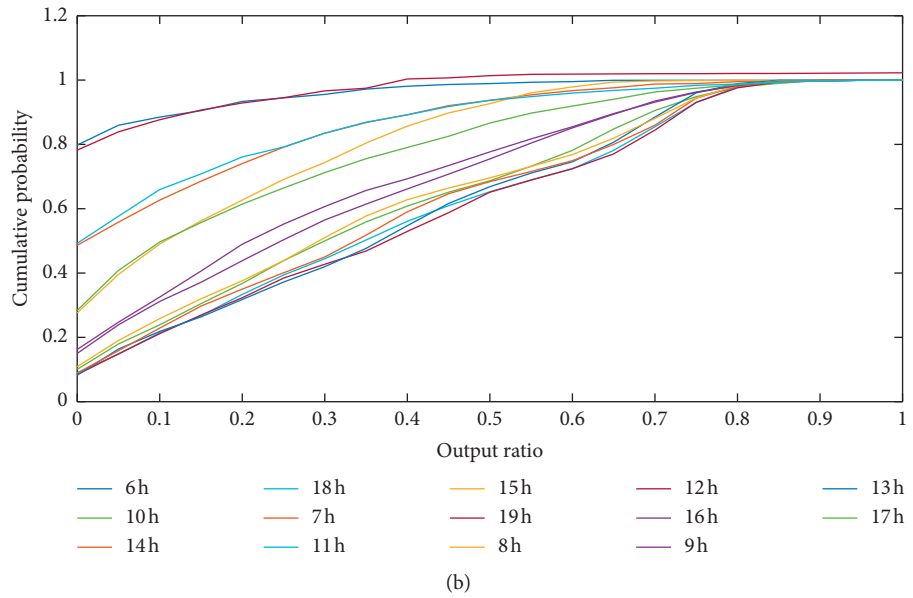

(b)

Figure 6: Output probability and cumulative probability for different time periods.

Table 2: Correlation between wind and photovoltaic power output in different seasons.

Parameters	Spring	Summer	Autumn	Winter
τ	0.0328	−0.0123	−0.0683	−0.0320
λ	0.0209	−0.0078	−0.0435	−0.0204

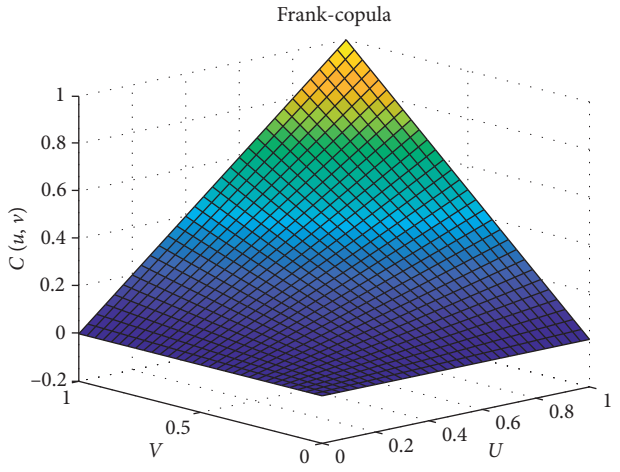

Figure 7: Joint probability distribution of the wind-photovoltaic output.

and the heater was placed horizontally in the oil shale layer so that the layer absorbed most of the heat and not much heat loss occurred. Due to the complexity of the shale's endothermic mechanism, underground heat conduction, and other loss factors, the heat loss of the heating medium differs for different time periods; therefore, a small random fluctuation is added to the heating power as an adjustment.

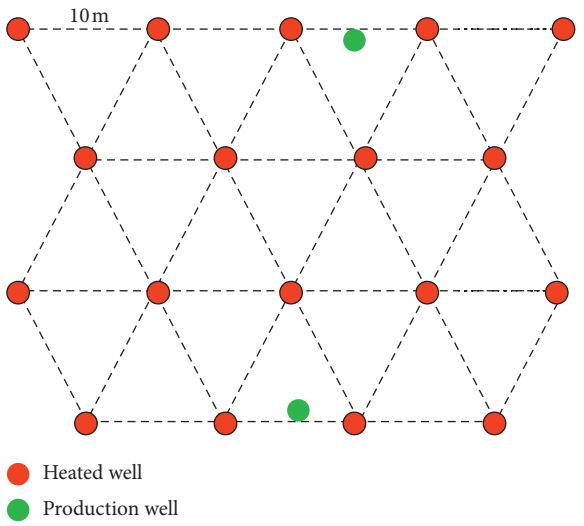

Figure 8: Diagram of the well network.

Figure 11 shows the load power required for heating the oil shale in 24 hours.

6. Optimization Strategy and Economic Analysis

As shown in Figure 10, when the oil shale is heated to 450°C, the oil yield of the shale is 90%. An economic analysis and optimization of the case were conducted. The oil shale is heated until the temperature reaches 450°C; this is followed by cooling and reheating to 450°C. A PSO algorithm is used to optimize the heating temperature of the heated well. The objective is to minimize the cost. A simulation is conducted for different power supply combinations.

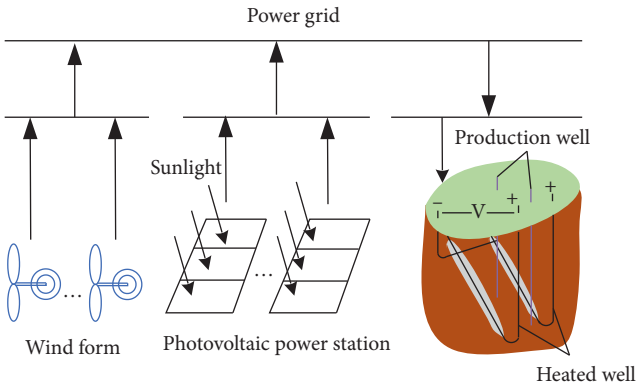

Figure 9: Diagram of in-situ oil shale exploitation with wind and photovoltaic energy.

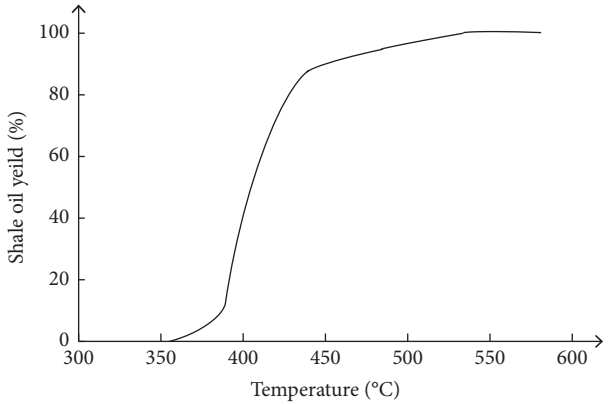

Figure 10: Relationship between the oil yield and heating temperature.

6.1. Particle Swarm Optimization. PSO was proposed by Eberhart and Kennedy in 1995 based on the theory of artificial life and evolutionary computation. The concept is based on the foraging behavior of birds. In PSO, the solution of each optimization problem is a bird in the search space, which is called a "particle." Each particle has an initial velocity and position, and an adaptive value is determined by the fitness function. Each particle is endowed with a memory function that remembers the best location to search and the speed of each particle determines the direction and distance to fly so that the particle can search in the optimal solution space.

In the optimization process of each iteration, the particle updates its speed and position by comparing the fitness value and two extreme values, i.e., the optimal solution (individual extreme value $X\text{best}_i$) found by the particle itself and the optimal solution (global extreme value $X\text{best}_g$) found by the whole population, namely,

$$\begin{aligned} v_{\text{in}}(t+1) &= v_{\text{in}}(t) + c_1 r_1 \left[X\text{best}_{\text{in}} - x_{\text{in}}(t)\right] \\ &\quad + c_2 r_2 \left[X\text{best}_{\text{gn}} - x_{\text{in}}(t)\right], \\ x_{\text{in}}(t+1) &= x_{\text{in}}(t) + v_{\text{in}}(t+1), \end{aligned} \tag{10}$$

where t is the number of iterations; $v_{\text{in}}(t)$ is the velocity of the ith particle in the t iteration; $X\text{best}_i$ is the optimal individual history location of particle i; $X\text{best}_g$ is the optimal position of the group history; $x_{\text{in}}(t)$ is the position of the particle in t iterations; c_1 represents the cognitive factor; and c_2 represents the social factor and the acceleration weight. Usually $c_1 = c_2 = 2$; in fact, the acceleration weight can be changed; r_1 and r_2 are random variables between 0 and 1.

The PSO algorithm has been used by many scholars because it has a simple concept, easy implementation, fast convergence, and high efficiency; the method has been widely used in optimization problems in various engineering fields. In this study, the objective is to minimize the heating cost. Due to different reheating temperatures, the heating power required by the system will change, i.e., the cost will be different. In order to comprehensively consider the shale oil yield and the heating cost, PSO is used to optimize the reheating temperature of the heated well.

6.2. Scheduling Strategy. The scheduling strategy of the combined wind-solar power supply is formulated according to the known data of the wind farm power output, curtailed wind power output, photovoltaic power output, and curtailed photovoltaic power output, and the simulation is conducted. In general, the energy scheduling strategy of the combined wind-solar power supply system is based on the following principles:

(1) When the total power output of the wind-solar power generation system is large and a certain amount of curtailed wind power and curtailed photovoltaic power are generated, it is preferred to use the cheaper curtailed wind power and curtailed photovoltaic power to supply power to the load.

(2) When the total power output of the wind-solar power generation system is small and curtailed wind power and curtailed photovoltaic power are not generated, the power will be purchased directly from the grid to meet the load demand.

6.3. Economic Analysis. Data from Jilin are used as the example; the on-grid price of photovoltaic power is 0.65 yuan/kW·h, and the curtailed photovoltaic power price is 0.325 yuan/kW·h. The contract price of curtailed wind power signed with the wind farm is 0.2617 yuan/kW·h, and the transmission and distribution cost of the power grid company is 0.11 yuan/kw·h. The time-of-use price of electricity purchased from the grid is shown in Table 4.

Based on this electricity price, we establish economic models of five power supply modes for comparison:

Mode 1: the electricity needed to heat the shale comes entirely from the grid.

Mode 2: based on the curtailed wind electricity price of 0.3717 yuan/kW·h (contract, transmission, and distribution), the heating power required for oil shale exploitation is completely obtained from the curtailed wind power, and it is assumed that the curtailed wind power fully meets the load.

Table 3: Heating index for the heat absorption efficiency values of 0.7 and 0.6

	Temperature (°C)	Required heat Q(J)	Time t(h)
Heat absorption efficiency is 0.7	12–450	6.8766 ∗ 1013	3032.01
	450–400	7.85 ∗ 1012	807.61
	400–450	7.85 ∗ 1012	346.12
Heat absorption efficiency is 0.6	12–450	6.8766 ∗ 1013	3537.35
	450–400	7.85 ∗ 1012	605.71
	400–450	7.85 ∗ 1012	403.81

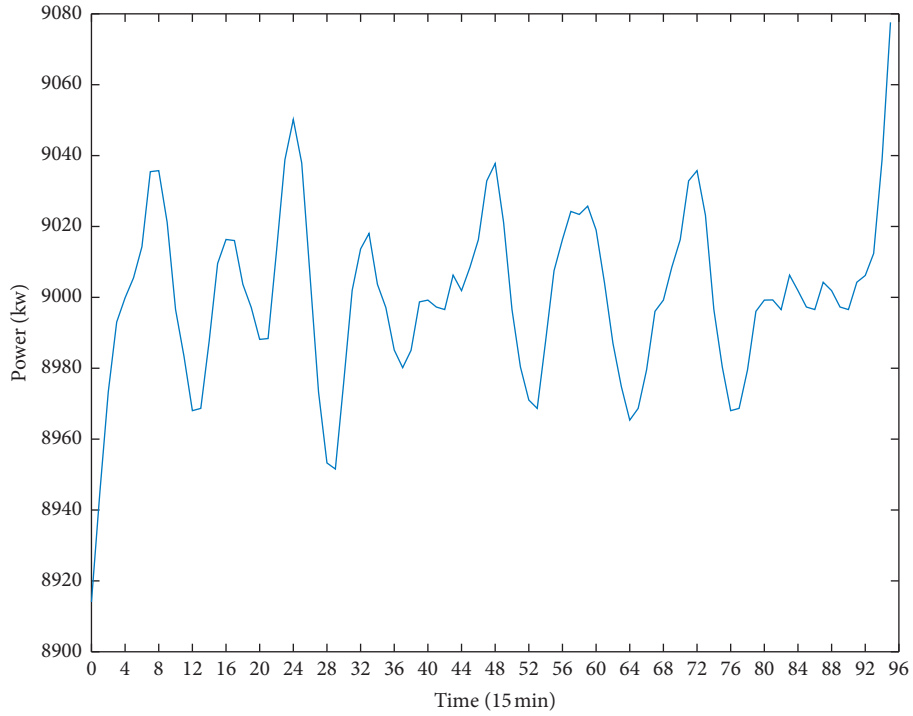

Figure 11: Load power during the 24 h heating process.

Table 4: Time-of-use price.

	Peak	Flat	Valley
Time slot	8 : 00–12 : 00 14 : 00–21 : 00	5 : 00–8 : 00 12 : 00–14 : 00 21 : 00–00 : 00	00 : 00–5:00
Price/yuan	0.80405	0.5497	0.329

Mode 3: based on the curtailed photovoltaic electricity price of 0.325 yuan/kW·h, the heating power required for oil shale exploitation is completely obtained from the curtailed photovoltaic power, and it is assumed that the curtailed photovoltaic power fully meets the load.

Mode 4: the heating power required for oil shale exploitation can be selected from the grid, the curtailed wind power, and the curtailed photovoltaic power at any time, and it is assumed that the curtailed wind power and curtailed photovoltaic power meet the load.

Mode 5: considering the configuration capacity constraints of wind power and photovoltaic power, the maximum output coefficient of wind power is 0.56–0.7, and the maximum output of photovoltaic power at any time should not exceed $P_{\text{pv max}}$, which should satisfy:

$$\begin{aligned} &P_{\text{pv}}(t) < P_{\text{pv max}}, \\ &P_{\text{pv max}} = P_{w\max} - \left(P_{w\max} \times 0.7\right), \end{aligned} \tag{11}$$

where $P_{\text{pv}}(t)$ is the photovoltaic power output at time t; $P_{\text{pv max}}$ is the maximum power output of the photovoltaic power station; and $P_{w\max}$ is the maximum transmission power of the wind farm. Since large power consumption enterprises generally have a direct agreement price with wind farms and photovoltaic power stations, the price for wind power is 0.3717 yuan/kW·h, and the price for photovoltaic power is 0.325 yuan/kW·h.

6.3.1. Electricity Cost. The results of the PSO of the electricity cost in the mining cycle for the five modes are shown in Table 5.

Figure 12 shows the electricity cost of the five modes for the heat absorption rates of 0.6 and 0.7.

Table 5: Comparison of the electricity costs for the five modes.

Mode	Heat absorption efficiency	Optimum temperature (°C)	Electricity cost/yuan
1	0.6	430	109,198,463.80
	0.7	430	84,868,246.94
2	0.6	430	65,434,056.91
	0.7	430	50,888,690.87
3	0.6	430	57,212,990.30
	0.7	430	44,495,088.87
4	0.6	430	60,785,323.67
	0.7	430	47,269,772.97
5	0.6	430	98,123,390.22
	0.7	430	76,633,371.28

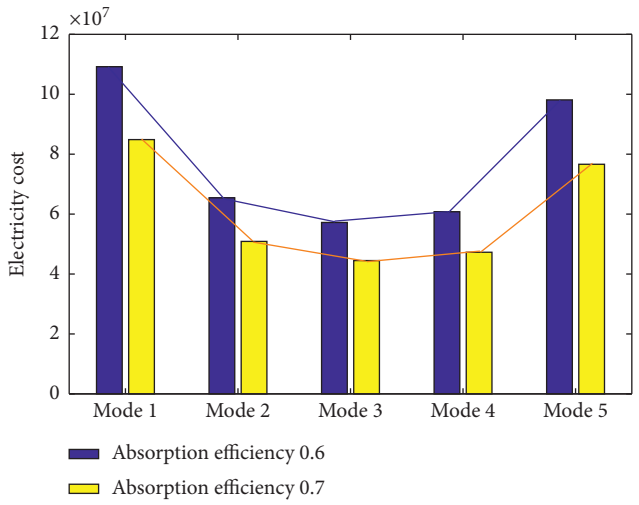

Figure 12: Electricity cost for different heat absorption rates.

Figure 12 shows that for the heat absorption rate of 0.7, Mode 5 has the highest electricity cost because all the electricity for heating is purchased from the grid, which is expensive. Mode 4 has the second highest electricity price because the configuration capacity constraints of wind power and photovoltaic power are considered. Mode 3 has the lowest electricity cost. However, due to intermittent photovoltaic power generation, there is no photovoltaic power output at night. Therefore, the electricity cost of Mode 3 is 44,495,088.87 yuan, which is an ideal value and cannot be achieved in practice. Compared with the aforementioned three schemes, Mode 4 with the second-low-price and Mode 2 with the third-low-price have feasibility for practical engineering. The results indicate that the electricity cost is higher for the lower heat absorption efficiency for all modes. Mode 1 has the largest difference in electricity cost (24,330,216.86 yuan), and Mode 3 has the smallest difference (12,717,901.43 yuan). These results provide guidance for decision-makers to dispatch the power for the exploitation of oil shale.

6.3.2. Profit Analysis. We use the current market price of shale oil of an oil shale company in Jilin province at 4100 yuan/ton as an example; the ratio of the income to electricity cost is obtained as follows:

Table 6: The ratio of profit and electricity cost for the five modes.

Mode	Profit/Electricity cost	
	Heat absorption efficiency is 0.7	Heat absorption efficiency is 0.6
1	4.78	3.71
2	7.97	6.20
3	9.11	7.09
4	8.58	6.67
5	5.29	4.13

$$S = \frac{P_c \cdot Q}{P_e}, \tag{12}$$

where P_c is the price of shale oil (4100 yuan/ton); Q is the annual tonnage of shale oil; and P_e is the annual electricity bill. According to the mining scale of the project and the geological characteristics of the oil shale, the tonnage of shale oil extracted during the mining cycle is 98,910 tons; therefore, the profit $P = P_c \times Q = 40,553,100$ yuan.

Using the results in Table 5, the income from the shale oil is calculated, and an economic analysis is conducted. Table 6 shows the ratio of the profit and electricity cost of the five modes.

The results show that the system has the lowest return for Mode 1, but the ratio is close to the current international shale oil yield ratio, which is in line with the actual situation. If the resources of curtailed wind power, curtailed photovoltaic power, and other resources can be used during the mining process, the electricity cost of mining oil shale can be reduced. Therefore, it is evident that the combined wind-solar power for the power supply of oil shale in-situ mining can improve the profit of the enterprise. The results of this study provide guidance for power supply planning and the design of in-situ oil shale mining projects.

7. Conclusions

In this study, the characteristics of the power output of wind farms and photovoltaic power stations and their correlation are analyzed. It is concluded that photovoltaic output is strongly correlated with time, wind power output is weakly correlated with time, and wind power output is not correlated with photovoltaic power output in the study area. The objective was to minimize the cost of a given oil shale

load, and a PSO algorithm was used to optimize the heating temperature of the heated well. An economic analysis of five different power supply combinations with wind power, photovoltaic power, and the power grid was conducted for in-situ exploitation of oil shale, and the cost/benefit ratios of the five modes were obtained. The simulation results indicate that it is feasible to use wind power and photovoltaic power as a heating power source at the right price for in-situ exploitation of shale oil. The results provide valuable reference data for decision makers to plan and design the power supply for in-situ exploitation of oil shale projects using electric heating.

Data Availability

The wind and solar data used to support the findings of this study are available from the corresponding author upon request. The data on oil shale used to support the findings of this study are included within the article.

Conflicts of Interest

The authors declare that they have no conflicts of interest.

Acknowledgments

The authors would like to appreciate the funding support from the State Energy Center for Shale Oil Research and Development (grant no. G5800-18-ZS-KFNY005); the National Natural Science Foundation of China (grant no. 51677067); and the Fundamental Research Funds for the Central Universities (grant no. 2018MS27).

References

[1] Y. Kang, "Significant exploration progress and resource potential of unconventional oil and gas in China," *Oil Forum*, vol. 37, no. 4, pp. 1–7, 2018.

[2] S. Hu, C. Xiao, X. Liang, Y. Cao, X. Wang, and M. Li, "The influence of oil shale in situ mining on groundwater environment: a water-rock interaction study," *Chemosphere*, vol. 228, pp. 384–389, 2019.

[3] R. Liu, "Development direction and trend of oil shale mining technology," *Value Engineering*, vol. 37, no. 18, pp. 240-241, 2018.

[4] Z. Yang, J. Zhu, X. Li, D. Luo, S. Qi, and M. Jia, "Experimental investigation of the transformation of oil shale with fracturing fluids under microwave heating in the presence of nanoparticles," *Energy & Fuels*, vol. 31, no. 10, pp. 10348–10357, 2017.

[5] J. Zhu, Z. Yang, X. Li, S. Qi, and M. Jia, "Application of microwave heating with iron oxide nanoparticles in the in-situ exploitation of oil shale," *Energy Science & Engineering*, vol. 6, no. 5, pp. 548–562, 2018.

[6] J. Zhu, Z. Yang, X. Li, N. Wang, and M. Jia, "Evaluation of different microwave heating parameters on the pore structure of oil shale samples," *Energy Science & Engineering*, vol. 6, no. 6, pp. 797–809, 2018.

[7] C. Gao, J. Su, Y. Wang, X. Meng, Y. Wang, and L. Zhang, "Research progress of numerical simulation on oil shale in-situ production," *Oil Drilling & Production Technology*, vol. 40, no. 3, pp. 330–335, 2018.

[8] J. X. Ma, L. F. Xue, J. M. Zhao, and F. T. Bai, "Numerical simulation and design optimization of temperature field of oil shale in situ pyrolysis and exploitation," *Science Technology and Engineering*, vol. 19, no. 5, pp. 94–103, 2019.

[9] W. Sheng, M. Wu, J. Yu et al., "Key techniques and engineering practice of distributed renewable generation clusters integration," *Proceedings of the CSEE*, vol. 39, no. 8, pp. 2175–2186, 2019.

[10] F. Pilo, G. Pisano, and G. G. Soma, "Advanced DMS to manage active distribution network," in *Proceedings of the IEEE Bucharest Power Tech Conference*, Bucharest, Romania, 2009.

[11] C. Xu, L. Liu, and Y. Xie, "Real-time data based online evaluation of output performance for wind turbine units," *Thermal Power Generation*, vol. 44, no. 4, pp. 88–91, 2015.

[12] M. Chao, Z. Mi, and Z. Weiji, "The optimal control and simulation of MPPT for photovoltaic cells generation system," *Computer Simulation*, vol. 36, no. 3, pp. 128–132, 2019.

[13] Q. Zhou, N. Wang, R. Liang et al., "Analysis of the causes of China's new energy abandoning the wind and abandoning the light," *Electric Power*, vol. 49, no. 9, 2016.

[14] National Energy Administration, *China's Wind Power Grid Operation in the First Half of 2015*, National Energy Administration, Beijing, China, 2015.

[15] National Energy Administration, *Wind Power Industry Monitoring*, National Energy Administration, Beijing, China, 2014.

[16] State Electricity Regulatory Commission, *Wind Power Consumption Regulatory Report in Key Areas*, State Electricity Regulatory Commission, Beijing, China, 2011.

[17] National Energy Administration, *Photovoltaic Power Generation Construction Information in the First Half of 2015*, National Energy Administration, Beijing, China, 2015.

[18] Z. Bie, G. Hu, H. Xie, and G. Li, "Optimal dispatch for wind farm power integrated systems considering demand response," *Automation of Electric Power Systems*, vol. 38, no. 13, pp. 115–120, 2014.

[19] G. E. Jia-yun, "Multi-objective optimization method for source and load of power system considering wind power consumption," *Telecom Power Technology*, vol. 35, no. 7, pp. 70-71, 2018.

[20] D. Zeng, J. Yao, S. Yang et al., "Optimization dispatch modeling for price-based demand response considering security constraints to accommodate the wind power," *Proceedings of the CSEE*, vol. 34, no. 31, pp. 5571–5578, 2014.

[21] Y. Xu, X. Yan, R. Li, T. Li, and H. Zeng, "Active and reactive power joint optimization of active distribution network with "generation-grid-load-energy storage" interaction in power market environment," *Power System Technology*, vol. 43, no. 10, pp. 3778–3789, 2019.

[22] X. Yang, H. Liu, and Q. Huang, "Optimal dispatching model of wind-sunlight-storage combining with "peak shaving" considering time-of-use electricity price," *Acta Energiae Solaris Sinica*, vol. 39, no. 6, pp. 1752–1760, 2018.

[23] S. Kang, J. Li, Y. Li, J. Zhu, B. Liang, and M. Liu, "Multi-objective generation scheduling model of source and load considering the strategy of TOU price," *Power System Protection and Control*, vol. 44, no. 11, pp. 83–89, 2016.

[24] L. Riboldi and L. Nord, "Offshore power plants integrating a wind farm: design optimisation and techno-economic assessment based on surrogate modelling," *Processes*, vol. 6, no. 12, p. 249, 2018.

[25] H. Daneshi and A. K. Srivastava, "Security-constrained unit commitment with wind generation and compressed air

energy storage," *IET Generation, Transmission & Distribution*, vol. 6, no. 2, pp. 167–175, 2012.

[26] Z. Wang, J. Li, Z. Xu, and C. Wan, "Study on load-grid-generation coordination method and accommodation increment assessment based on synchronization consumptive of abandoned wind power and solar," *Renewable Energy Resources*, vol. 34, no. 10, pp. 1441–1448, 2016.

[27] L. Hui, H. Gao, Y. Zhang, and A. Xin, "Expansion planning of large scale hybrid wind-photovoltaic transmission network considering correlation," *Power System Technology*, vol. 42, no. 7, pp. 2120–2127, 2018.

[28] S. Song, *Copulas Function and its Application in hydrology*, Science Press, Beijing, China, 2012.

[29] C. Fang, D. Zheng, and Z. Ge, "Shell ICP technology field test," *Science and Technology Innovation Herald*, vol. 36, pp. 110-111, 2010.

[30] M. S. K. Youtsos and E. Mastorakos, "Numerical simulation of thermal and reaction waves for in situ combustion in hydrocarbon reservoirs," *Fuel*, vol. 108, pp. 780–792, 2013.